

## Upper limit of two-dimensional hole gas mobility in strained Ge/SiGe heterostructures

T. Tanaka, Y. Hoshi, K. Sawano, N. Usami, Y. Shiraki et al.

Citation: *Appl. Phys. Lett.* **100**, 222102 (2012); doi: 10.1063/1.4723690

View online: <http://dx.doi.org/10.1063/1.4723690>

View Table of Contents: <http://apl.aip.org/resource/1/APPLAB/v100/i22>

Published by the [American Institute of Physics](#).

---

### Related Articles

Comment on "Intrinsic point defect incorporation in silicon single crystals grown from a melt, revisited" [*J. Appl. Phys.* **110**, 063519 (2011)]

[J. Appl. Phys.](#) **111**, 116102 (2012)

Shape evolution in glancing angle deposition of arranged Germanium nanocolumns

[J. Appl. Phys.](#) **111**, 104309 (2012)

Dopant effects on the photoluminescence of interstitial-related centers in ion implanted silicon

[J. Appl. Phys.](#) **111**, 094910 (2012)

Nano-electron beam induced current and hole charge dynamics through uncapped Ge nanocrystals

[Appl. Phys. Lett.](#) **100**, 163117 (2012)

Experimental and theoretical analysis of the temperature dependence of the two-dimensional electron mobility in a strained Si quantum well

[J. Appl. Phys.](#) **111**, 073715 (2012)

---

### Additional information on *Appl. Phys. Lett.*

Journal Homepage: <http://apl.aip.org/>

Journal Information: [http://apl.aip.org/about/about\\_the\\_journal](http://apl.aip.org/about/about_the_journal)

Top downloads: [http://apl.aip.org/features/most\\_downloaded](http://apl.aip.org/features/most_downloaded)

Information for Authors: <http://apl.aip.org/authors>

## ADVERTISEMENT

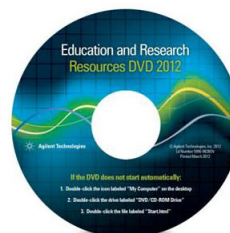


**Agilent Technologies**

### Agilent Education and Research Resources DVD 2012

Packed with over **100 NEW** articles, application notes, webcasts, and videos relating to Renewable Energy, Nanoscience, RF/Wireless, MIMO, Materials, Digital Signals, Photonics, and General Test & Measurement.

[Click Here to  
Order Your DVD](#)



Agilent Technologies

# Upper limit of two-dimensional hole gas mobility in strained Ge/SiGe heterostructures

T. Tanaka,<sup>1</sup> Y. Hoshi,<sup>2</sup> K. Sawano,<sup>3</sup> N. Usami,<sup>2</sup> Y. Shiraki,<sup>3</sup> and K. M. Itoh<sup>1,a)</sup>

<sup>1</sup>*School of Fundamental Science and Technology, Keio University, 3-14-1 Hiyoshi, Kohoku-ku, Yokohama 223-8522, Japan*

<sup>2</sup>*Institute for Materials Research, Tohoku University, 2-1-1 Katahira, Aoba-ku, Sendai 980-8577, Japan*

<sup>3</sup>*Research Center for Silicon Nano-Science, Advanced Research Laboratories, Tokyo City University, 8-15-1 Todoroki, Setagaya-ku, Tokyo 158-0082, Japan*

(Received 10 April 2012; accepted 11 May 2012; published online 30 May 2012)

High two-dimensional hole gas (2DHG) mobility ( $\mu_{2\text{DHG}} > 10000 \text{ cm}^2/\text{Vs}$  at  $T < 100 \text{ K}$ ) strained Ge/Si<sub>1-x</sub>Ge<sub>x</sub> structures with  $x = 0.5$  and  $0.65$  were fabricated, and temperature dependence of their 2DHG mobility was obtained experimentally by the mobility spectrum analysis of the conductivity under magnetic fields. The theoretically calculated 2DHG mobility was compared to experimental data to determine the effective deformation potentials for scattering by acoustic and optical phonons. Using empirically confirmed parameters, the upper theoretical limit of room temperature 2DHG mobility  $\mu_{2\text{DHG}}$  in strained Ge as a function of strain was calculated. The possibility to achieve  $\mu_{2\text{DHG}} > 5000 \text{ cm}^2/\text{Vs}$  at room temperature is presented. © 2012 American Institute of Physics. [<http://dx.doi.org/10.1063/1.4723690>]

Two-dimensional hole gas (2DHG) formed in a strained Ge layer grown on a Si<sub>x</sub>Ge<sub>1-x</sub> virtual substrate has high 2DHG hole mobility  $\mu_{2\text{DHG}}$  because of the reduction in the effective hole mass and suppression of the interband scattering thanks to strain modification of the valence band structure. Up to now,  $3100 \text{ cm}^2/\text{Vs}$  is the highest mobility reported for room temperature.<sup>1</sup> Although this hole mobility is about 150% and 700% higher than those in bulk Ge and Si, respectively, the theoretical limit of  $\mu_{2\text{DHG}}$  in the Ge/Si<sub>1-x</sub>Ge<sub>x</sub> heterostructure has not been established due to the experimental challenge of measuring purely the 2DHG mobility and theoretical challenge of modeling it with the anisotropy and nonparabolicity of the valence band included appropriately. Indeed, a previously reported determination of the “2DHG mobility” had employed a simple Hall measurement detecting not purely the mobility of the 2DHG but also of the modulation-doped layer, i.e., the resulting mobility was given as the average of the two.<sup>2</sup> Therefore, their results for the room temperature 2DHG mobility were only an approximation. The previous calculations were also approximations based on simple parabolic subband structures.<sup>2-4</sup> In this study, we obtain pure 2DHG mobility by measuring the magnetic field dependence of Ge/Si<sub>1-x</sub>Ge<sub>x</sub> heterostructures and its analysis by maximum entropy mobility spectrum analysis (MEMSA).<sup>5</sup> Moreover, we theoretically reproduce the experimental 2DHG mobility based on subband structures obtained with the six-band **k**·**p** method including the anisotropy and nonparabolicity of the valence band. With such a combination of rigorous experimental and theoretical methods, we establish parameters for phonon and interface roughness scattering and demonstrate theoretically the upper limit of 2DHG mobility in Ge/Si<sub>1-x</sub>Ge<sub>x</sub> heterostructures.

Three p-type modulation doped Ge/SiGe heterostructures shown in Fig. 1 were employed in this work. Two of them were grown by solid source molecular beam epitaxy

(SS-MBE) on n-type Si(001) substrates. Strain-relaxed Si<sub>0.5</sub>Ge<sub>0.5</sub>/Si<sub>0.75</sub>Ge<sub>0.25</sub>/Si(001) buffer layers were grown by using two-step low-temperature-buffer technique,<sup>6</sup> and the roughness of the buffer layers was removed by chemical mechanical polishing.<sup>7,8</sup> Then a 50 nm Si<sub>0.5</sub>Ge<sub>0.5</sub> layer, a 10 nm boron-doped layer, a 10 nm spacer layer, a Ge channel, a 30 nm Si<sub>0.5</sub>Ge<sub>0.5</sub> layer, and a 3 nm Si cap layer were grown successively. The channel thickness and boron concentration of sample A were 7.5 nm and  $\sim 2 \times 10^{18} \text{ cm}^{-3}$ , and that of sample B were 20 nm and  $\sim 3 \times 10^{18} \text{ cm}^{-3}$ , respectively. The growth temperatures of Ge channels were 300 °C. Other sample C was grown by gas source-MBE (GS-MBE) and SS-MBE on n-type Si(001) substrate. Using the graded buffer technique,<sup>9</sup> a strain-relaxed Si<sub>0.35</sub>Ge<sub>0.65</sub> layer was grown by GS-MBE, and the roughness of the buffer layers was removed by chemical mechanical polishing<sup>7,8</sup> followed by a successive growth of a 50 nm Si<sub>0.35</sub>Ge<sub>0.65</sub> layer, a 20 nm Ge channel, and a 10 nm spacer layer. Then the sample was transferred to SS-MBE, and boron  $\delta$  doping ( $\sim 1 \times 10^{12} \text{ cm}^{-2}$ ) was performed followed by growth of a 30 nm Si<sub>0.2</sub>Ge<sub>0.8</sub> and a 3 nm Si cap layer. A standard Hall bar geometry was defined on the sample by optical lithography. Ohmic contacts were made by AuGa evaporation.

The following measurement schemes were performed to determine purely the 2DHG mobility excluding the conductivity component of the parallel boron-doped layer. The temperature dependence ( $T = 5\text{--}290 \text{ K}$ ) of magnetoresistance and Hall resistance of samples were measured in the magnetic field  $B$  between  $-9$  and  $+9 \text{ T}$  to determine the conductivity tensor components  $\sigma_{xx}(B)$  and  $\sigma_{xy}(B)$ . The temperature dependence of the 2DHG mobility and density was obtained from  $\sigma_{xx}(B)$  and  $\sigma_{xy}(B)$  by means of the maximum-entropy mobility spectrum analysis fit procedure.<sup>5</sup> Figures 2(a) and 2(b) show the temperature dependence of 2DHG mobility and density, respectively. 2DHG mobilities of the samples at 290 K were  $2440 \text{ cm}^2/\text{Vs}$  for sample A,  $2900 \text{ cm}^2/\text{Vs}$  for sample B, and  $3120 \text{ cm}^2/\text{Vs}$  for sample C. The mobility for

<sup>a)</sup>Electronic mail: kitoh@appi.keio.ac.jp.

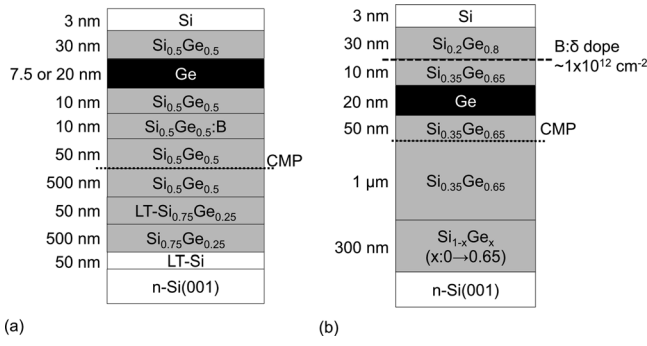


FIG. 1. Schematic diagrams of Ge/SiGe heterostructures: (a) 7.5 nm Ge and  $2 \times 10^{18} \text{ cm}^{-3}$  boron for sample A and 20 nm Ge and  $3 \times 10^{18} \text{ cm}^{-3}$  boron for sample B; (b) Sample C.

sample C has marked the highest experimental 2DHG mobility.<sup>1</sup> In addition, from the measurement of magnetoresistance, Shubnikov-de Haas oscillations were obtained to determine the roughness of the Ge/Si<sub>1-x</sub>Ge<sub>x</sub> interface.

In order to numerically reproduce the 2DHG mobility obtained by the experiments, subband structures and quantum well potentials were obtained by solving the six-band  $\mathbf{k} \cdot \mathbf{p}$  and Poisson's equations self-consistently as a function of the measured 2DHG density.<sup>10,11</sup> The set of valence band parameters employed in the calculation is shown in Table I. The  $xx$ -component of the 2DHG mobility was obtained from a linearization of the Boltzmann equation as<sup>10</sup>

$$\mu_{xx} = \frac{e}{4\hbar^2\pi^2k_B T n_{2\text{DHG}}} \sum_l \int_0^{2\pi} d\phi \int_{E_l^{(0)}}^{\infty} dE \frac{k_l(E, \phi)}{\left| \frac{\partial E_l}{\partial k} \right|_{k_l(E, \phi)}} \times \left( \frac{\partial E_l}{\partial k} \right)_{k_l(E, \phi)}^2 \tau_x^{(l)} [k_l(E, \phi), \phi] f_0(E) [1 - f_0(E)], \quad (1)$$

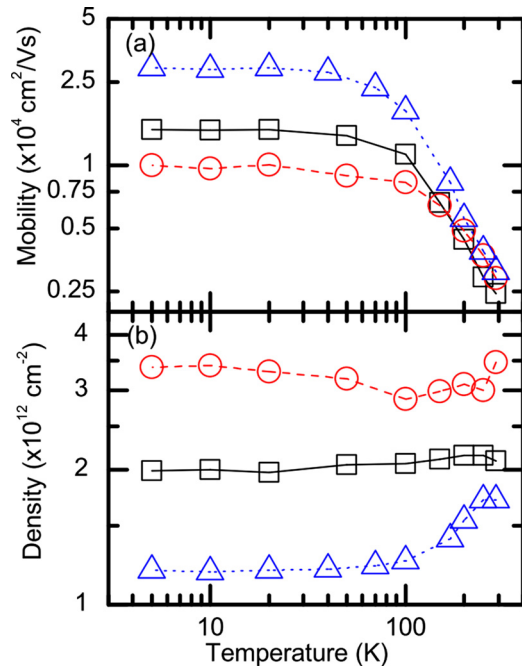


FIG. 2. Experimentally obtained 2DHG (a) mobility and (b) density for sample A ( $\square$  and solid curve), sample B ( $\circ$  and dashed curve), and sample C ( $\Delta$  and dotted curve). The curves are guide to eyes.

where  $n_{2\text{DHG}}$  is the 2DHG density,  $k_l$  is the in-plane wave-number at the energy  $E$ ,  $\phi$  is the in-plane polar angle in the  $l$ th subband,  $E_l^{(0)}$  is the energy of the  $l$ th subband at  $\mathbf{k}_l = 0$ ,  $\tau_x^{(l)}$  is the transport relaxation time for the  $x$  component in the  $l$ th subband, and  $f_0(E)$  is the Fermi-Dirac function. Scattering by acoustic phonons, optical phonons, remote ionized impurities, and interface roughness were included. Our samples contain  $10^6$ – $10^7 \text{ cm}^{-2}$  threading dislocations. That may act as scattering centers. However, based on Eqs. (1) and (5) and the number of traps per length of dislocation  $N_T = 10^6 \text{ cm}^{-1}$  given in Ref. 15, we found the threading dislocation limited mobility  $\mu_{\text{th}} \geq 10^8 \text{ cm}^2/\text{Vs}$  i.e., scatterings caused by threading dislocations can be neglected. The relaxation times for the acoustic and optical phonon scattering were computed with the isotropic approximation as<sup>11</sup>

$$\frac{1}{\tau_{x,\text{AP}}^{(l)}(k)} = \frac{k_B T D_{\text{AP}}^2}{2\pi\hbar\rho u_l^2} \sum_m \int d^2\mathbf{k}' \delta[E_m(\mathbf{k}') - E_l(\mathbf{k})] F_{lm}, \quad (2)$$

$$\frac{1}{\tau_{x,\text{OP}}^{(l)}(k)} = \frac{D_{\text{OP}}^2}{4\pi\rho\omega_{\text{OP}}} \sum_m \int d\mathbf{k}' \delta[E_m(\mathbf{k}') - E_l(\mathbf{k}) \mp \hbar\omega_{\text{OP}}] \times F_{lm} \frac{1 - f_0[E_l(\mathbf{k}) \mp \hbar\omega_{\text{OP}}]}{1 - f_0[E_l(\mathbf{k})]} \left( n_{\text{OP}} + \frac{1}{2} \pm \frac{1}{2} \right), \quad (3)$$

where  $\rho$  is the mass density,  $u_l$  is the longitudinal sound velocity,  $\omega_{\text{OP}}$  is the frequency of the optical phonon,  $\delta$  is the Dirac delta function,  $D_{\text{AP}}$  is the effective deformation potential of the acoustic phonon,  $D_{\text{OP}}$  is the effective deformation potential of the optical phonon,  $n_{\text{OP}}$  is the Bose occupation factor of optical phonons, and  $F_{lm}$  is the form factor described as

$$F_{lm} = \int dz |\psi_0^{(l)}(z) \cdot \psi_0^{(l)\dagger}(z)|^2, \quad (4)$$

where  $\psi_0^{(l)}$  is the wave function of  $l$ th subband at  $\mathbf{k} = 0$ . While values of deformation potentials for the strain Ge reported previously in the literature scatter significantly,<sup>12,16–18</sup> the best agreement between the experimental results and the calculation was obtained with the effective deformation potentials of acoustic phonon  $D_{\text{AP}} = 6.65 \text{ eV}$  and optical phonon  $D_{\text{OP}} = 8.52 \times 10^8 \text{ eV/cm}$ . These numbers are consistent with the calculation in Ref. 19 based on the deformation potential parameters  $a$ ,  $b$ ,  $c$ , and  $d_0$  listed in Table I. The transport relaxation times for remote ionized impurities and interface roughness were calculated as follows. The dielectric screening was treated as in Refs. 10 and 20 with the isotropically approximated subband structure. From the doping condition of each sample, the transport relaxation time for remote ionized impurities for the in-plane wavenumber  $\mathbf{k}$  in the  $l$ th subband was calculated as

TABLE I. Valence band parameters and deformation potentials for Ge.

$L$ ( $\hbar^2/2m_0$ )	$M$ ( $\hbar^2/2m_0$ )	$N$ ( $\hbar^2/2m_0$ )	$a$ (eV)	$b$ (eV)	$d$ (eV)	$d_0$ (eV)
$-30.53^a$	$-4.64^a$	$-33.64^a$	$2.1^b$	$-1.87^b$	$-4.8^b$	$29.0^c$

<sup>a</sup>Reference 12.

<sup>b</sup>Reference 13.

<sup>c</sup>Reference 14.

$$\frac{1}{\tau_{x,\text{imp}}^{(l)}(\mathbf{k})} = \frac{1}{2\pi\hbar} \int dz N(z) \int d^2\mathbf{k}' \delta[E_l(\mathbf{k}') - E_l(\mathbf{k})] \times |v_{\text{imp}}^l(\mathbf{k}' - \mathbf{k}, z)|^2 (1 - \cos\theta), \quad (5)$$

where  $N(z)$  is the concentration of the ionized impurities,  $\mathbf{k}'$  is the in-plane wavenumber of the final state,  $\theta$  is the scattering angle formed by  $\mathbf{k}'$  and  $\mathbf{k}$ , and  $v_{\text{imp}}^l(\mathbf{k}' - \mathbf{k})$  is the matrix element for remote ionized impurities with Eq. (4.18) in Ref. 21. The intersubband scattering was neglected. The transport relaxation time for interface roughness scattering was calculated as

$$\frac{1}{\tau_{x,\text{IR}}^{(l)}(\mathbf{k})} = \frac{\Delta^2 \Lambda^2}{2\hbar} \sum_m \int d^2\mathbf{k}' \frac{\delta[E_m(\mathbf{k}') - E_l(\mathbf{k})]}{[1 + \Lambda^2(\mathbf{k}' - \mathbf{k})^2/4m]^{n+1}} \times |M_{\text{IR}}^m(\mathbf{k}' - \mathbf{k})|^2 (1 - \cos\theta), \quad (6)$$

where  $\Delta$  is the root-mean-square of the roughness height,  $\Lambda$  is the in-plane correlation length of the roughness,  $n = 4$  is an exponent describing the falloff of the distribution for large  $(\mathbf{k}' - \mathbf{k})$ ,<sup>22,23</sup> and  $M_{\text{IR}}^m(\mathbf{k}' - \mathbf{k})$  is the matrix element for the interface roughness with Eq. (31) in Ref. 24. The same values of  $\Delta$  and  $\Lambda$  were employed for the top and bottom interfaces. To determine  $\Delta$  and  $\Lambda$ , the Dingle ratio  $\alpha$  (the ratio between transport relaxation time and single-particle relaxation time) and experimentally obtained 2DHG mobility were used. Dingle ratios  $\alpha = 11.0$  for sample A,  $\alpha = 5.1$  for sample B, and  $\alpha = 4.6$  for sample C were obtained from the magnetic field dependence of Shubnikov-de Haas oscillations.<sup>25,26</sup> Then the values of  $\Delta$  and  $\Lambda$  were found self-consistently to satisfy the experimental Dingle ratio and 2DHG mobility.  $\Delta$  and  $\Lambda$  determined in this manner were  $\Delta = 0.74$  nm and  $\Lambda = 19$  nm for sample A,  $\Delta = 0.52$  nm and  $\Lambda = 12.5$  nm for sample B, and  $\Delta = 0.43$  nm and  $\Lambda = 12$  nm for sample C. These values were in good agreement with  $\Lambda = 20 - 30$  nm found by the cross-sectional transmission electron microscope images of a typical Ge/Si<sub>x</sub>Ge<sub>1-x</sub> heterostructure.<sup>27</sup> Parameters employed for mobility calculation are summarized in Table II.

Figs. 3(a)–3(c) show comparison between experimentally measured and theoretically calculated 2DHG mobility. Excellent agreements with the experimental 2DHG mobility demonstrate the validity of our calculation. Figure 3 shows convincingly that the interface roughness scattering is the limiting factor below 200 K and its effect is still significant at room temperature even in sample C, which has the highest experimental 2DHG mobility.

It is possible to reduce the interface roughness and remote ionized impurities scattering in the future by improving the sample fabrication technique. Thus, the upper theoretical limit of 2DHG mobility will be limited by acoustic and optical phonon scattering. Figure 4 shows calculated room-temperature ( $T = 290$  K) 2DHG mobility as a function of a Ge composition  $x$  for a relaxed Si<sub>1-x</sub>Ge<sub>x</sub> buffer layer when the interface roughness and remote ionized impurities are removed completely ( $\Delta = 0$  and  $\Lambda = 0$ ). Here, 2DHG density dependence is also shown since the density changes the position of the Fermi level which in turn changes the effective mass due to the strong nonparabolicity of the

TABLE II. Scattering parameters.

	Sample A	Sample B	Sample C
$D_{\text{AP}}$ (eV)	6.65	6.65	6.65
$D_{\text{OP}}$ ( $10^8$ eV/cm)	8.52	8.52	8.52
$\Delta$ (nm)	0.74	0.52	0.43
$\Lambda$ (nm)	19	12.5	11

valence band. The calculation is performed for 20 nm thick strained Ge layers, whose thickness is large enough to sustain the form factor. When the thickness is reduced, the form factor is increased leading to reduction in the 2DHG mobility. A doping layer to supply holes to the well is assumed to situate above the channel. Figure 4 suggests that the room temperature mobility of  $\sim 3000$  cm<sup>2</sup>/Vs in Fig. 2 can be increased up to more than 5000 cm<sup>2</sup>/Vs if the roughness is removed and the 2DHG concentration is tuned appropriately.

In conclusion, we have obtained purely the 2DHG mobility in three Ge/Si<sub>1-x</sub>Ge<sub>x</sub> heterostructures by the mobility spectrum analysis of the magnetic field dependence of their

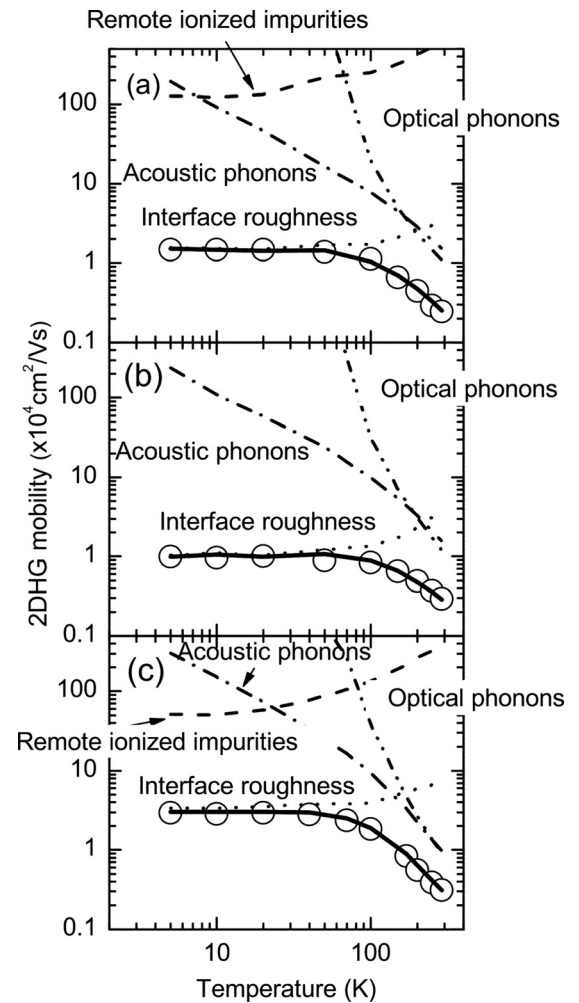


FIG. 3. Comparison between experimental ( $\circ$ ) and theoretically calculated (solid curves) 2DHG mobility for (a) sample A, (b) sample B, and (c) sample C. Contributions of acoustic phonon scattering (dashed-dotted curves), optical phonon scattering (dashed-two dotted curves), remote ionized impurity scattering (dashed curves), and interface roughness scattering (dotted curves) are shown.

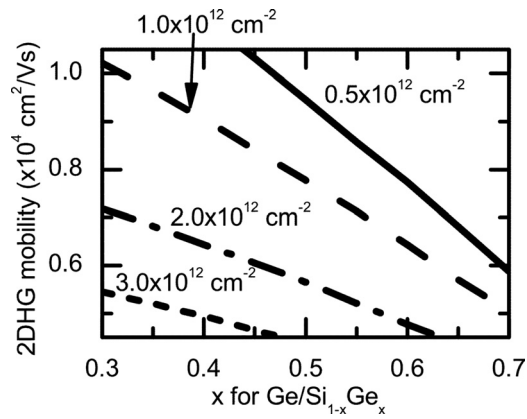


FIG. 4. Phonon-limited 2DHG mobility in strained Ge on relaxed  $\text{Si}_{1-x}\text{Ge}_x$  heterostructure with different 2DHG densities.

conductivity. The 2DHG mobilities were reproduced very well by the calculation based on the Boltzmann equation and subband structures obtained by the six-band  $\mathbf{k}\cdot\mathbf{p}$  method. The acoustic phonon, optical phonon, remote ionized impurity, and interface roughness scatterings were included. Finally, the upper limit of 2DHG mobility in strained Ge limited by acoustic and optical phonon scattering was evaluated as a function of the composition  $x$  in the underlying substrate  $\text{Si}_{1-x}\text{Ge}_x$ . The possibility to achieve  $\mu_{2\text{DHG}} > 5000 \text{ cm}^2/\text{Vs}$  at room temperature was shown.

The work at Keio has been supported in part by the Grant-in-Aid for Scientific Research and Project for Developing Innovation Systems by MEXT, FIRST, and CREST-JST. The work at Tokyo City University has been supported by Project for strategic advancement of research infrastructure for private universities 2009-2013, by Grant-in-Aid for Scientific Research from MEXT, Japan, and by Industrial Technology Research Grant Program from NEDO.

- <sup>1</sup>M. Myronov, K. Sawano, Y. Shiraki, T. Mouri, and K. M. Itoh, *Appl. Phys. Lett.* **91**, 082108 (2007).
- <sup>2</sup>S. Madhavi, V. Venkataraman, and Y. H. Xie, *J. Appl. Phys.* **89**, 2497 (2001).
- <sup>3</sup>M. Myronov, T. Irisawa, S. Koh, O. A. Mironov, T. E. Whall, E. H. C. Parker, and Y. Shiraki, *J. Appl. Phys.* **97**, 083701 (2005).
- <sup>4</sup>B. Laikerman and R. A. Kiehl, *Phys. Rev. B* **47**, 10515 (1993).
- <sup>5</sup>S. Kiatgamolchai, M. Myronov, O. A. Mironov, V. G. Kantser, E. H. C. Parker, and T. E. Whall, *Phys. Rev. E* **66**, 036705 (2002).
- <sup>6</sup>M. Myronov, T. Irisawa, O. A. Mironov, S. Koh, Y. Shiraki, T. E. Whall, and E. H. C. Parker, *Appl. Phys. Lett.* **80**, 3117 (2002).
- <sup>7</sup>K. Sawano, K. Kawaguchi, S. Koh, Y. Shiraki, Y. Hirose, T. Hattori, and K. Nakagawa, *J. Electrochem. Soc.* **150**, G376 (2003).
- <sup>8</sup>K. Sawano, Y. Abe, H. Satoh, K. Nakagawa, and Y. Shiraki, *Jpn. J. Appl. Phys., Part 2* **44**, L1320 (2005).
- <sup>9</sup>E. A. Fitzgerald, Y.-H. Xie, M. L. Green, D. Brasen, A. R. Kortan, J. Michel, Y.-J. Mii, and B. E. Weir, *Appl. Phys. Lett.* **59**, 811 (1991).
- <sup>10</sup>M. V. Fischetti, Z. Ren, P. M. Solomon, M. Yang, and K. Rim, *J. Appl. Phys.* **94**, 1079 (2003).
- <sup>11</sup>Y. Zhang, M. V. Fischetti, B. Sorée, W. Magnus, M. Heyns, and M. Meuris, *J. Appl. Phys.* **106**, 083704 (2009).
- <sup>12</sup>M. V. Fischetti and S. E. Laux, *J. Appl. Phys.* **80**, 2234 (1996).
- <sup>13</sup>J.-M. Jancu and P. Voisin, *Phys. Rev. B* **76**, 115202 (2007).
- <sup>14</sup>F. Cerdeira and M. Cardona, *Phys. Rev. B* **5**, 1440 (1972).
- <sup>15</sup>L. M. Giovane, H.-C. Luan, A. M. Agarwal, and L. C. Kimerling, *Appl. Phys. Lett.* **78**, 541 (2001).
- <sup>16</sup>L. Reggiani, C. Canali, F. Nava, and G. Ottaviani, *Phys. Rev. B* **16**, 2781 (1977).
- <sup>17</sup>K. Takeda, A. Taguchi, and M. Sakata, *J. Phys. C* **16**, 2237 (1983).
- <sup>18</sup>T. Yamada and D. K. Ferry, *Solid-State Electron.* **38**, 881 (1995).
- <sup>19</sup>M. Costato and L. Reggiani, *Phys. Status Solidi B* **58**, 471 (1973).
- <sup>20</sup>M. V. Fischetti, *J. Appl. Phys.* **89**, 1232 (2001).
- <sup>21</sup>T. Ando, A. B. Fowler, and F. Stern, *Rev. Mod. Phys.* **54**, 437 (1982).
- <sup>22</sup>R. M. Feenstra, M. A. Lutz, F. Stern, K. Ismail, P. M. Mooney, F. K. LeGoues, C. Stanis, J. O. Chu, and B. S. Meyerson, *J. Vac. Sci. Technol. B* **13**, 1608 (1995).
- <sup>23</sup>D. N. Quang, N. H. Tung, D. T. Hien, and T. T. Hai, *J. Appl. Phys.* **104**, 113711 (2008).
- <sup>24</sup>D. Monroe, Y. H. Xie, E. A. Fitzgerald, P. J. Silverman, and G. P. Watson, *J. Vac. Sci. Technol. B* **11**, 1731 (1993).
- <sup>25</sup>P. T. Coleridge, R. Stoner, and R. Fletcher, *Phys. Rev. B* **39**, 1120 (1989).
- <sup>26</sup>See supplementary material at <http://dx.doi.org/10.1063/1.4723690> for the determination of the Dingle ratio from Shubnikov-de Haas oscillations.
- <sup>27</sup>K. Sawano, K. Toyama, R. Masutomi, T. Okamoto, N. Usami, K. Arimoto, K. Nakagawa, and Y. Shiraki, *Appl. Phys. Lett.* **95**, 122109 (2009).